Physical Coupling Fusion Sensing of MFL-EMAT for Synchronous Surface and Internal Defects Inspection

Qin Tang, Bin Gao, *Senior Member, IEEE*, Gaige Ru, Guixin Qin, Wai Lok Woo, *Senior Member, IEEE*, Shiqiang Jiang, Dajiang Chen, Jingwei Li, and Ju Cheng

***Abstract*—Nondestructive testing (NDT) techniques are widely used for inspection and evaluation of conductive materials. However, a single physical mechanism sensing cannot simultaneously satisfy multiple inspection requirements. In this article, we propose a hybrid transducer based on magnetic flux leakage (MFL) and electromagnetic acoustic transducer (EMAT) for synchronous detection of surface and internal defects. In the proposed hybrid transducer, both MFL and EMAT share a common magnetic field. The magnetic circuit characteristics of the MFL and EMAT principles are fully exploited, and the magnetic field provided by a single permanent magnet is used to excite ultrasonic waves that can detect internal defects within the sample. Iron is used to introduce a magnetic field into the sample and provide a horizontal magnetic field to detect discontinuities on the near surface of the sample. The huge frequency difference between the MFL signal and the EMAT signal effectively suppresses interference between the two signals. Simulations and experiments have been undertaken to show that the proposed transducer can overcome the detection limitations associated with the MFL and the dead detection zone of the EMAT while simultaneously detecting surface defects, internal defects, and bottom thinning defects in the specimen.**

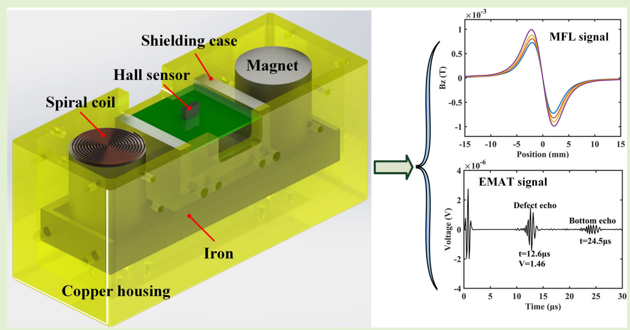

***Index Terms*— Magnetic flux leakage–electromagnetic acoustic transducer (MFL-EMAT), multiphysics fusion, surface and internal defects, synchronous detection.**

I. Introduction

METAL materials are widely used in pipelines, railway transportation, aerospace, nuclear industry, and so on. The pits, corrosion, and slag inclusion in the infrastructure have become the main source of accidents. Under the influence of high temperature, high pressure, and alternating stress, these defects will form creep and fatigue damage, leading to serious accidents such as material leakage and even explosion. Therefore, nondestructive evaluation (NDE) and structural health monitoring (SHM) are essential for metal materials.

Nondestructive testing (NDT) methods include ultrasonic testing (UT), acoustic emission (AE) testing, magnetic flux leakage (MFL) testing, magnetic particle testing (MT), penetration testing (PT), alternating current field measurement (ACFM), eddy current testing (ECT), radiography, and fiber optics [1]. Radiography and fiber optics systems are costly and require specialized equipment to be preinstalled in the inspection environment [2]. MT and PT are easy to implement, whereas pretreatment for the specimen surface is required to be done before detection, which is not suitable for online inspection [3]. ECT is sensitive to surface defects and does not need to remove the coating layer. ACFM can provide the defect length and depth, while they are mainly used for surface and near-surface defect detection due to the skin effect [4], [5], [6]. Multifrequency eddy current and pulsed eddy current have been shown to carry rich defect information, while the signal processing and analysis issues remain

Manuscript received 27 April 2023; accepted 16 May 2023. Date of publication 2 June 2023; date of current version 14 July 2023. This work was supported in part by the National Natural Science Foundation of China under Grant 61971093, Grant 61960206010, and Grant 61527803; in part by the Deyuan and University of Electronic Science and Technology of China (UESTC) Joint Research Center; in part by the Science and Technology Department of Sichuan, China, under Grant 2019YJ0208, Grant 2018JY0655, and Grant 2018GZ0047; and in part by the Fundamental Research Funds for the Central Universities under Grant ZYGX2019J067. The associate editor coordinating the review of this article and approving it for publication was Dr. Kagan Topalli. *(Corresponding author: Bin Gao.)*

Please see the Acknowledgment section of this paper for the author affiliations.

This article has supplementary downloadable material available at https://doi.org/10.1109/JSEN.2023.3280670, provided by the authors.

Digital Object Identifier 10.1109/JSEN.2023.3280670

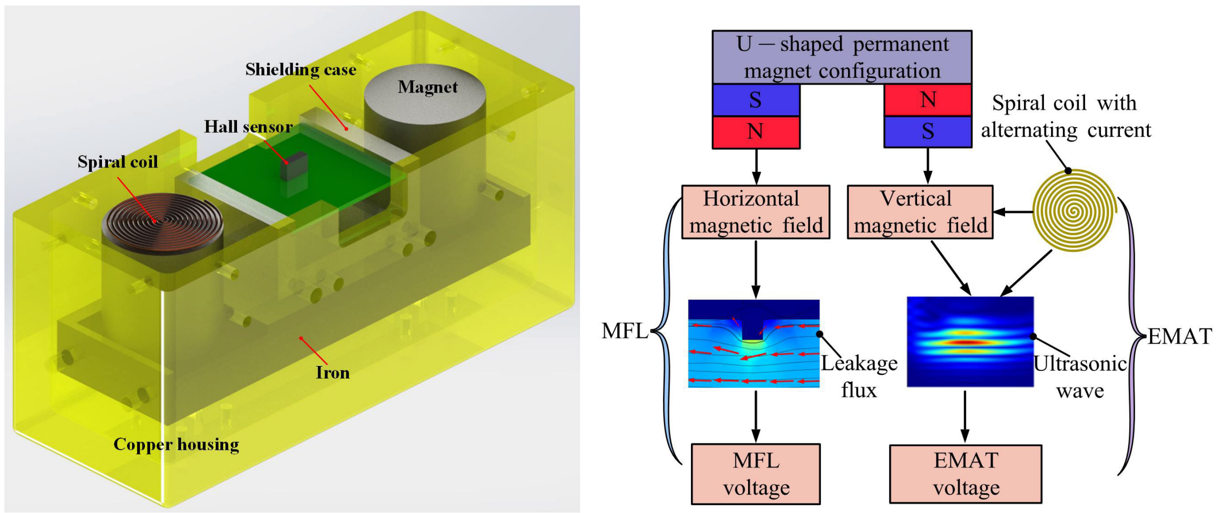

(a) (b)

Fig. 1. Schematic of the structure and fusion method of the hybrid transducer. (a) Sensing structure. (b) Fusion method.

challenging [7]. MFL can be used for deeper detection depth than ECT and ACFM, where it has been widely employed in oil and gas pipeline inspection. Unfortunately, MFL signals are susceptible to movement speed (e.g., on pipeline pig), and defects that are parallel to the magnetization direction are difficult to be identified [8]. UT is widely used for internal flaw detection because of its good penetration. The traditional piezoelectric transducer (PZT) has a good signal-to-noise ratio (SNR), and however, it requires a couplant between the sample and the transducer. In addition, for particular inspection environments, such as curved surface and narrow inspection space, it requires wedge blocks to meet the adaptive requirement of various natural shapes of the testing specimen [9]. Electromagnetic acoustic transducers (EMATs) generate ultrasonic wave by electromagnetic coupling [10]. However, the applications of EMAT are limited due to its lower conversion efficiency and poor SNR [11]. In addition, the dead zone brought by near-field emission is more serious than PZT, which means that defects in the near-field region cannot be efficiently detected. This phenomenon is particularly evident when the bulk wave is employed for detection.

It should be noted that each NDT method has its advantages and limitations. For a single NDT method, it is difficult to satisfy different locations and types of flaws detection in a specimen. To increase the sensitivity and reliability of the detection system, recent research has focused on multiphysics sensing mechanisms and structures to obtain more defect information [12], [13], [14]. Chang et al. [15] proposed a magnetoelectric–ultrasonic hybrid transducer that combines with ACFM and dual piezoceramic UT mechanism. When the bipulse signal with different pulsewidths is used to excite the hybrid transducer, it can simultaneously detect surface and internal defects in metal. Ru et al. [16] presented a new electromagnetic coupling structure integrating ACFM and MFL sensing mechanisms. This structure is capable of detecting flaws in different directions as well as surface and subsurface defects. Mishakin et al. [17] used a dual system of individual UT and ECT to assess loading-induced damage in austenitic steel. By measuring the coil impedance near the resonant frequency, Yin et al. [18] separated the capacitive and inductive effects of a coil. This method makes it possible to distinguish defects in the "insulator–conductor" structure. Subsequently, they combined capacitive sensing and electromagnetic induction, enabling the sensor to work in capacitive or inductive mode via phase switching. It has been successfully applied to the detection of composite materials in the "insulator–conductor" structure [19]. Li et al. [20] designed a multiphysics structured detection system, and the sensor consists of an L-shaped yoke surrounding an array of coils. The advantages of eddy current and eddy current thermography complement each other to increase the detectability of omnidirectional cracks. By applying a square-wave alternating magnetic field with dc bias to an electromagnetic sensor, the external defect in the ferromagnetic steel pipes can be effectively detected [21]. Li et al. [22] found the sensitivity of ACFM to arbitrary-angle defects can also be improved using a rotating magnetic field induced with an orthogonal excitation signal. By investigating the conductivity and permeability of special materials, the sensitivity of sensors can also be enhanced. For example, Chu et al. [23], [24] developed a low-power eddy current magnetoelectric sensor, the sensor utilized a composite material (FeBSi alloy Metglas) as a coupling medium and the power consumption of the sensor is as low as 0.625 μW. Liang et al. [25] reduced the influence of the liftoff distance on EMAT transduction efficiency by coating the stainless steel surface with Fe_3O_4, and the ultrasonic wave could be generated even at 8-mm liftoff.

As EMAT depends on electromagnetic induction, the feasibility of the ECT/EMAT fusion detection method has been demonstrated [26], [27], [28], [29]. Xie et al. [30] and Liu et al. [31] used a pulsed eddy current testing (PECT)/EMAT fusion detection method to detect metal material, the excitation is a half-sinusoidal signal, where ultrasonic wave and eddy current signal were separated from the

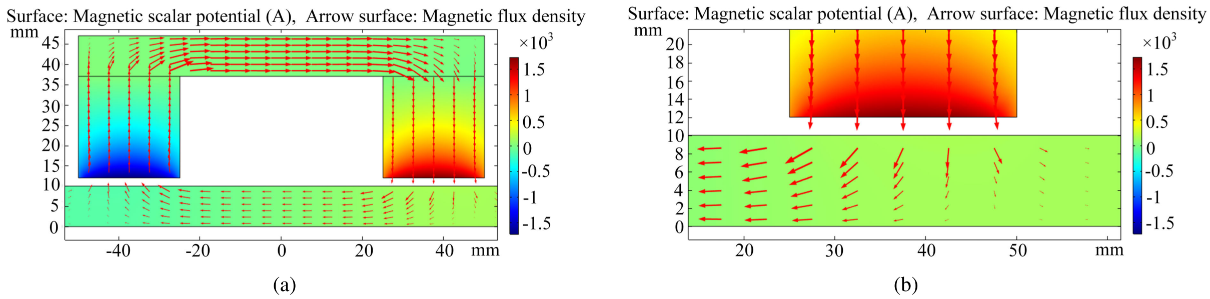

Fig. 2. Distribution of static magnetic field with U-shape configuration. (a) Whole view. (b) Partial view.

testing signal through the filtering strategy. However, when a sinusoidal pulse signal is used in EMAT, the frequency of the ultrasonic wave is mainly determined by the eddy current frequency (when the static magnetic field is provided by a permanent magnet), which means that the ECT signal frequency is significant close to the ultrasonic wave, and it is difficult to separate the signals from the time-domain perspective.

In this article, we propose a physical coupling fusion sensing of MFL-EMAT for both surface cracks and internal defects detection synchronously. The proposed transducer combines the advantages of MFL and EMAT, which overcomes the dead zone in the EMAT and the detection depth limitation in the MFL. Experiments and simulations have shown that the proposed structure can simultaneously detect surface and internal defects without significant interference between the MFL and EMAT signals.

The rest of this article is organized as follows. Section II introduces the theoretical analysis of the proposed hybrid transducer. Section III implements the numerical simulation. Section IV is carried out experimental verification by the proposed sensing structure. Finally, Section V concludes this article.

II. Methodology

A. Configuration of the Designed Hybrid Transducer

The proposed configuration of the MFL-EMAT transducer is shown in Fig. 1(a), and the fusion principle is shown in Fig. 1(b). Both EMAT and MFL share a common U-shaped excitation structure where the bias magnetic field in the EMAT is provided by the MFL configuration. For the MFL configuration, the magnetic field provided by the permanent magnets is introduced into the specimen through the iron, which magnetizes the specimen horizontally, as shown in Fig. 2(a). The shielding case prevents the sensor from being magnetized to saturation by the surrounding magnetic field, and the MFL signal is picked up by the highly sensitive Hall effect sensor placed in the middle of the U-shaped configuration. However, due to the limitations of magnetizing strength and specimen thickness, MFL is only suitable for surface and near-surface defect detection. For the EMAT configuration, a single permanent magnet provides a magnetic field perpendicular to the surface of the specimen, as shown in Fig. 2(b). This magnetic field interacts with the alternating eddy currents to excite the ultrasonic wave, and a spiral coil is used to excite and receive the ultrasonic wave. Ultrasonic wave is suitable for internal defects detection, especially when the specimen has a large thickness. Furthermore, the dead zone for near-surface detection caused by near-field emission in the EMAT can be supplied by MFL. In this way, the proposed fusion detection method based on MFL-EMAT can overcome the dead zone in EMAT and drawbacks in MFL, which can be used for both surface defect detection and internal defect detection simultaneously.

B. Mathematical Model of MFL in Fusion Structure

Fig. 3(a) shows the structure of the MFL testing device, which consists of iron, a pair of permanent magnets, and a sensor. Iron and permanent magnets form a U-shaped configuration, which is used to create a uniform horizontal magnetic field in the sample. The sample is excited to a saturated (or near saturated) magnetization state by this horizontal magnetic field. If there is a discontinuity in the sample surface, the magnetic flux will be "squeezed" into the air due to the low permeability of the discontinuity. Magnetic sensors [such as Hall effect sensor, giant magnetoresistance (GMR), and tunnel magnetoresistance (TMR)] are used to collect the leakage flux. Fig. 3(b) shows the equivalent magnetic circuit, and according to Kirchhoff's law, the flux and the reluctance in the equivalent magnetic circuit are given by [32]

$$\begin{cases} \phi_m = \phi_a + \phi_l + \phi_s \\ 2F_m = \phi_m R_m + \phi_a R_a \\ \phi_l R_l - R_a \phi_a = 0 \\ \left(R_g + R_s\right)\phi_s - \phi_l R_l = 0 \end{cases} \tag{1}$$

where, ϕ_a, ϕ_l, and ϕ_s are the magnetic flux of air between two magnet poles, leakage magnetic flux, and sample, respectively; ϕ_m is the main magnetic flux provided by permanent magnets; F_m denotes the magnetomotive force of permanent magnets; R_a and R_m represent the magnetoresistance of air between two magnet poles, permanent magnets and iron, respectively; and R_l, R_g, and R_s are the magnetoresistance of discontinuity part, gap, and sample, respectively.

The reluctance (R_{th}) of each part in the magnetic circuit is given in the following equation:

$$R_{\mathrm{th}} = \frac{l}{\mu S_a} \tag{2}$$

where l is the length of the magnetic flux path, μ is the permeability of the material, and S_a is the cross-sectional area of the magnetic flux path.

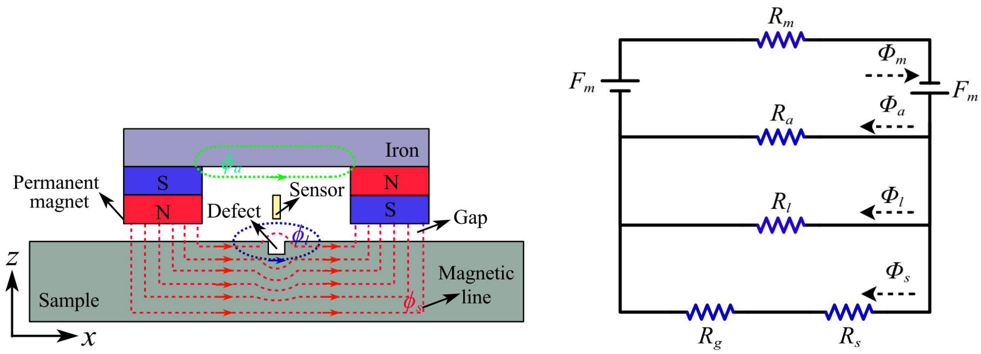

(a) (b)

Fig. 3. Working principle of MFL detection. (a) Excitation configuration of MFL. (b) Equivalent magnetic circuit.

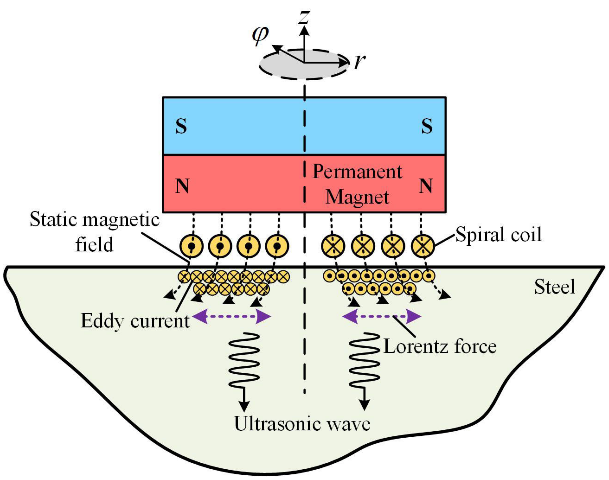

Fig. 4. Conversion mechanism of bulk-wave EMAT.

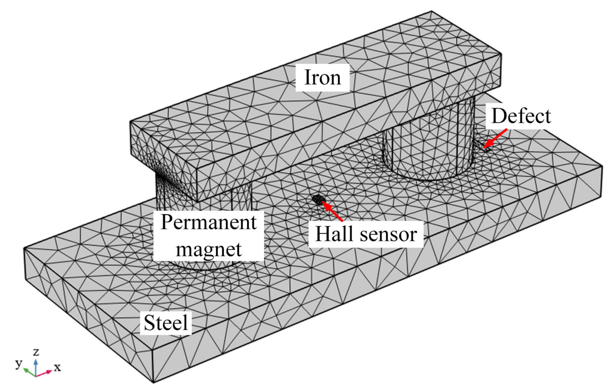

Fig. 5. Finite-element model of MFL.

C. Mathematical Model of EMAT in Fusion Structure

The conversion efficiency of EMAT includes Lorentz force, magnetostriction force, and magnetization force. When the permanent magnet is magnetized in the vertical direction (i.e., the bias magnetic field provided by the permanent magnet is mainly perpendicular to the sample), the magnetostriction force and magnetization force are quite small [33], [34]. In this article, we are mainly concerned with the mechanism of EMAT based on the Lorentz force. As shown in Fig. 4, when the alternating current is applied to the coil, an eddy current is induced in the near surface of the sample because of the skin effect. Meanwhile, the coil itself will also generate a dynamic magnetic field (DMF). The eddy current interacts with the static magnetic field and DMF will produce the Lorentz force and ultrasonic wave in the specimen.

The static magnetic field provided by the permanent magnet can be listed as follows [35]:

$$\boldsymbol{B}_s = \mu \boldsymbol{H} + \boldsymbol{B}_r \tag{3}$$

where $\boldsymbol{H}$ is the static magnet field intensity and μ and $\boldsymbol{B}_r$ are the relative permeability and residual magnetic flux density of the magnet, respectively.

The Lorentz force $\boldsymbol{f}_L$ produced by the interaction of the static magnetic field and DMF with the eddy current $\boldsymbol{J}_e$ is shown in (4), and the propagation of the elastic wave is governed by (5) [36]

$$\boldsymbol{f}_L = \boldsymbol{J}_e \times (\boldsymbol{B}_s + \boldsymbol{B}_d) \tag{4}$$

$$\boldsymbol{f}_L + \nabla \cdot \boldsymbol{T} = \rho \frac{\partial^2 \boldsymbol{u}}{\partial^2 t} \tag{5}$$

where $\boldsymbol{B}_d$ is the dynamic magnet field, $\boldsymbol{T}$ is the stress tensor, ρ is the mass density, and $\boldsymbol{u}$ is the displacement vector.

When there is a defect in the sample, the ultrasonic wave will be reflected by the defect and finally received by the coil. The location of the defect h can be determined as follows:

$$h = \frac{1}{2} \boldsymbol{v} t \tag{6}$$

where $\boldsymbol{v}$ is the velocity of the ultrasonic wave and t is the time of defect echo.

III. Simulation and Analysis

The commercial finite-element (FE) model software COMSOL is used to verify the feasibility of the proposed MFL-EMAT fusion detection method. To reduce the calculation time and complexity of the model, first, a 3-D FE model for MFL is established, which is shown in Fig. 5. The "magnetic fields, no currents" in the ac/dc module is used to solve the FE results. Referring to the distribution of the magnetic flux in Fig. 2, a 2-D axisymmetric FE model for bulk-wave EMAT is built in Fig. 6(a). The model parameters are listed in Tables I and II.

TABLE I
DESIGN PARAMETERS OF THE FINITE-ELEMENT MODEL

MFL		EMAT	
Parameter	Value (mm)	Parameter	Value (mm)
Specimen (length×width×height)	160×60×10	Specimen (radius×height)	30×40
Iron (length×width×height)	105×25×10	Permanent magnet (radius×height)	15×10
Defect length	10	Wire radius	0.2
Defect height	2	Coil radius	10
Defect width	1, 1.5, 2, 2.5	Defect diameter	1.5, 2.5
Defect angle (°)	90	Defect depth	10, 20
Sensor lift-off	2	Coil lift-off	0.5

TABLE II
ELECTROMAGNETIC PARAMETERS OF THE FINITE-ELEMENT MODEL

Material	Relative permeability	Conductivity (S/m)
Permanent magnet	1.04	7.14×10^5
Coil	1	6.00×10^7
Steel	190	4.03×10^6
Iron	4000	0.1
Air	1	0

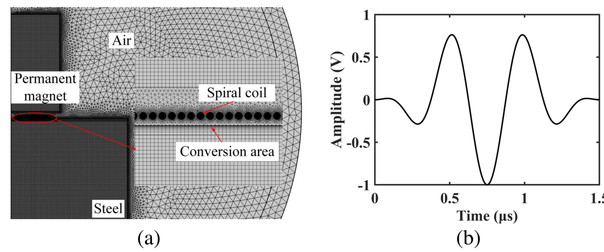

Fig. 6. (a) Finite-element model of bulk-wave EMAT. (b) Excitation signal.

The transient excitation current $i(t)$ of EMAT is expressed by

$$i(t)=\begin{cases} I_{\text{EMAT}}\left\{\cos(\bar{\omega}t)\left[1-\cos\left(\dfrac{\bar{\omega}t}{n}\right)\right]\right\}\Big/2 \\ \qquad 0\le t\le(2n\pi)/\bar{\omega} \\ 0,\quad t\ge(2n\pi)/\bar{\omega} \end{cases} \tag{7}$$

where I_{EMAT} is the magnitude of the excitation current and $\bar{\omega}=2\pi f$ is the angular center frequency. f and n are the excitation frequency and the number of cycles, and here, $f=2$ MHz and $n=3$. Fig. 6(b) shows the EMAT excitation signal in the simulation.

A. Simulation Results of Surface Defect Detection

Fig. 7 shows the magnetic flux distribution in the presence of defects on the surface of the sample, the permeability of the discontinuity is reduced, and the compressed magnetic field lines are squeezed into the air at the surface of the sample, creating a leakage flux.

In the MFL model, the defect angle is 90°. The length and depth of defects are 10 and 2 mm, respectively. The defect widths are 1, 1.5, 2, and 2.5 mm. Fig. 8(a) and (b) shows the simulation results for the horizontal magnetic field component Bx and the vertical magnetic field component Bz for different defect widths. As shown in Fig. 8(c) and (d), the amplitude of the Bx and Bz are increased nearly linearly to the defect width. When the defect width increases from 1 to 2.5 mm, Bx and Bz increase by 2.7% and 26.5%, respectively.

B. Simulation Results of Internal Defect Detection

Fig. 9 shows the propagation of the ultrasonic wave in the steel. It can be observed that the shear wave (S) and longitudinal wave (L) are generated simultaneously by the bulk-wave EMAT. The energy of the shear wave is stronger than that of the longitudinal wave, and the velocity of the longitudinal wave is faster than that of the shear wave. As shown in Fig. 9(b), the ultrasonic wave will be reflected when it encounters the defect, forming the defect echo.

TABLE III
DETECTION RESULTS WITH VARIOUS DEFECTS IN STEEL PLATE

Defect parameters				ΔBx voltage (V)	ΔBz voltage (V)
Defect angle (°)					
15	30	60	75	0.38, 0.41, 1.05, 0.95	0.63, 1.16, 1.36, 2.12
Length×width×depth: 20 mm × 3 mm × 2 mm					
Defect depth (mm)					
4	3	2	1	1.82, 1.46, 1.28, 0.89	2.64, 2.06, 1.68, 0.61
Length×width: 20 mm × 3 mm					
Defect length (mm)					
18	16	14	12	0.99, 0.95, 1.06, 0.71	1.51, 1.35, 1.10, 1.30
Width×depth: 3 mm × 2 mm					

In the EMAT model, blind holes are 1.5 and 2.5 mm in diameter and 10 and 20 mm in depth. Fig. 10 shows the induced voltage for the ultrasonic wave and the time of the defect echo. It can be seen from Fig. 10(a) that when a blind hole exists in the specimen, part of the ultrasonic energy is reflected by the bottom surface and another part is reflected by the defect (called defect echo). Fig. 10(b) shows the echo amplitude and time for blind holes of various depths and diameters. It can be seen from Fig. 10(b) that for defects with the same depth, a higher echo amplitude can be obtained for a defect with a larger diameter. This is attributed to the fact the energy of the reflected ultrasonic wave is determined by the defect area. Due to the negative correlation between defect echo distance and defect depth, a smaller echo time can be acquired for a deeper defect with the same diameter. According to the theory of ultrasonic wave propagation in solid, the defect location is determined by the time of defect echo [see (6)].

IV. EXPERIMENT

The experimental platform for the synchronous detection system is shown in Fig. 11. As shown in Fig. 11(a), the hybrid transducer consists of an EMAT coil, permanent magnets, iron,

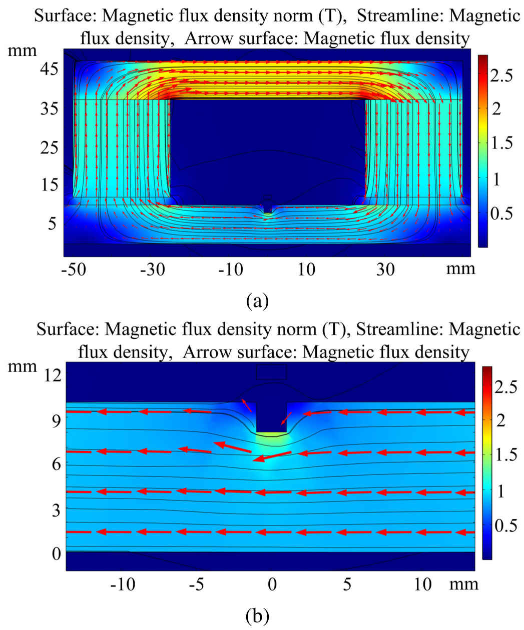

Fig. 7. Simulated results of magnetic field distribution in the sample. (a) Full view. (b) Partial view.

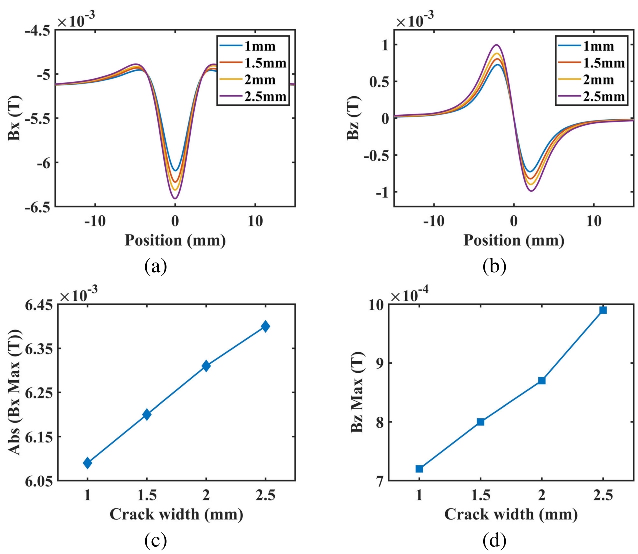

Fig. 8. Simulated results with different crack widths. (a) Bx. (b) Bz. (c) Abs (Bx max). (d) Bz max.

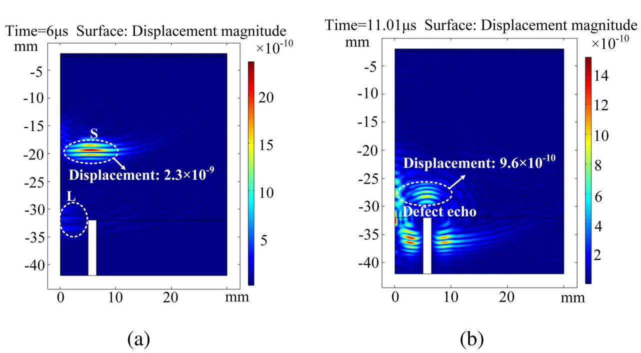

Fig. 9. Ultrasonic wave propagation in steel specimen. (a) 6 μs. (b) 11.01 μs.

Hall sensor, shielding case, and MFL signal detection circuit; all devices are packaged in a copper housing. To ensure the

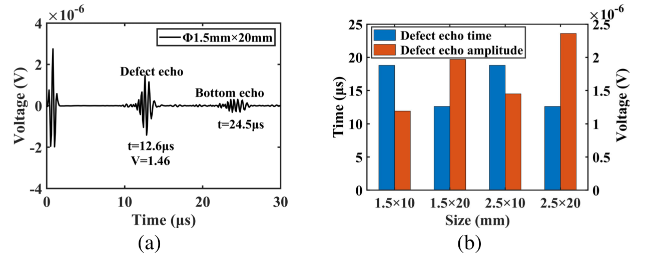

Fig. 10. Induced voltage signals with internal defect. (a) Φ1.5 $\times$ 20 mm. (b) Time and amplitude of defect echo.

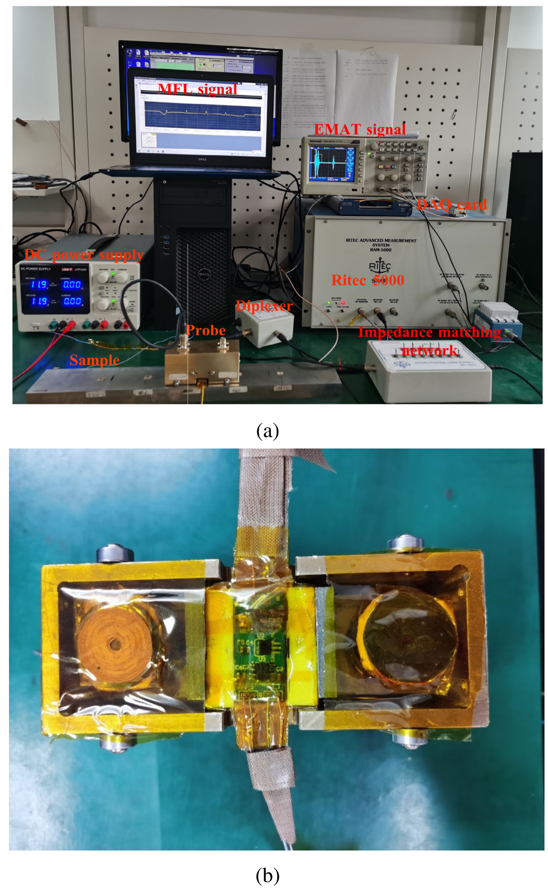

Fig. 11. Setup of experimental system. (a) MFL-EMAT synchronous detection system. (b) Hybrid transducer.

SNR of the MFL signal, high-sensitivity Hall sensor DRV 5055, low-noise operational amplifier AD620, and filtering circuit are integrated into the detection circuit. NI-6366 DAQ card is used for receiving MFL signals. The parameters of the permanent magnets and the iron are the same as in the simulation, and the sensor's liftoff is 2 mm.

EMAT shares a magnetic field with MFL; in addition, a burst signal with a frequency of 2 MHz and a duration of 1.5 μs is generated by a signal generator, and this burst signal is amplified by the power amplifier Ritec 5000 [see Fig. A1 in the Appendix (see the Supplementary Material)]. The amplified signal interacts with the magnetic field and generated the ultrasonic wave in the sample. Due to the lower conversion efficiency of the EMAT, the L-matching network is used to maximize the power transferred to the EMAT [35].

TABLE IV
DETECTION RESULTS OF SURFACE DEFECTS AND BOTTOM DEFECTS

Surface defect		Blind hole		
Size (mm) length×depth×width	ΔMFL voltage (V)	Size (mm) diameter×depth	Defect echo time (μs)	SNR (dB)
10×1×2.5	0.75	Φ7×20	14.2	20.5
10×1×2	0.72	Φ5×15	17.3	18.1
10×1×1.5	0.70	Φ7×10	20.4	21.1
10×1×1	0.63	Φ5×10	20.5	16.5

TABLE V
DETECTION RESULTS OF SURFACE DEFECTS AND BOTTOM THINNING DEFECTS

Surface defect		Bottom thinning defect		
Angle (°)	ΔMFL voltage (V)	Practical thickness (mm)	Measured thickness (mm)	Error (%)
75	1.89	23.35	24	2.7
60	1.63	19.36	20	3.2
45	1.30	15.52	16	3.0
30	1.27	11.56	12	3.6
15	0.96	/	/	/

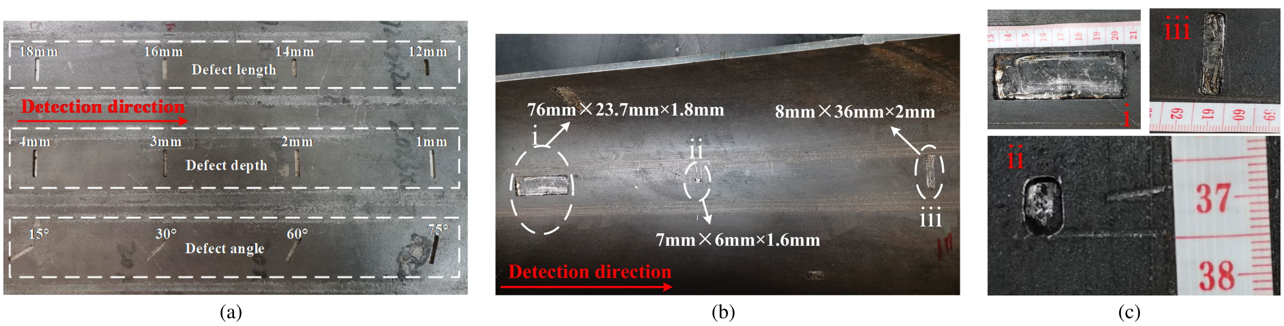

Fig. 12. Photographs of tested specimens with various defects. (a) Steel plate. (b) Pipeline. (c) Defects in pipeline.

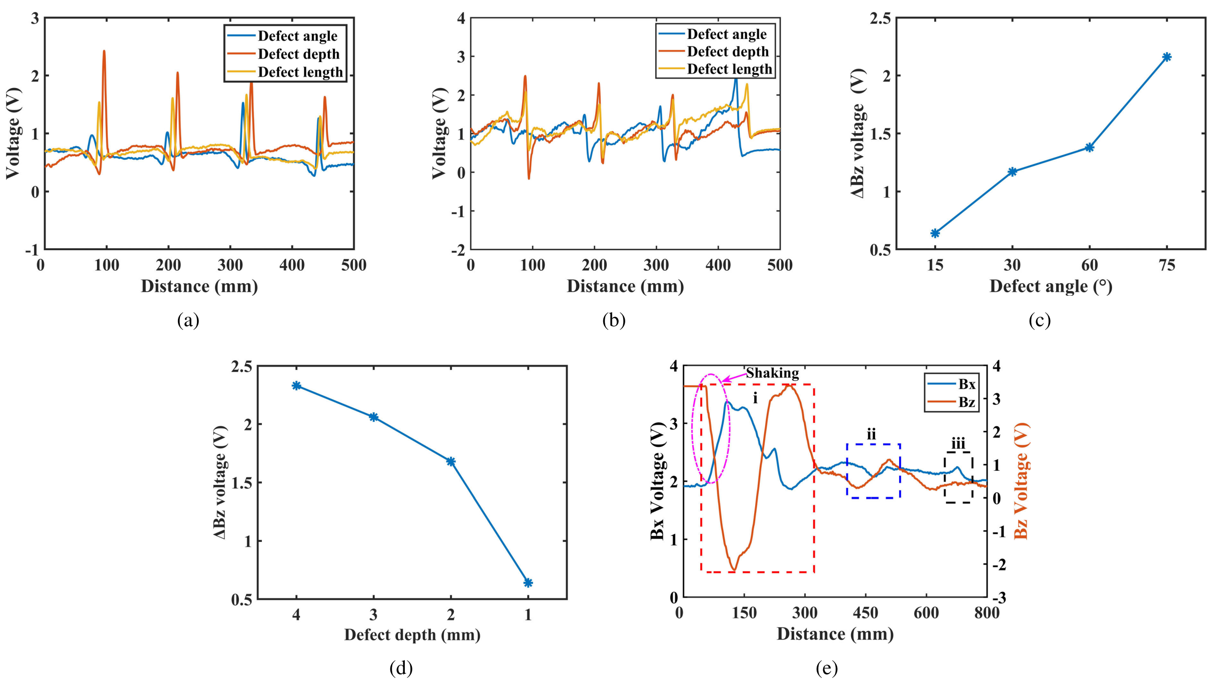

Fig. 13. Experimental results of MFL for different defects in steel plate and pipe. (a) Horizontal component Bx. (b) Vertical component Bz. (c) ΔBz voltage with different angles. (d) ΔBz voltage with different depths. (e) Detection results of defects in pipeline.

Oscilloscope is used to receive ultrasonic signals. The coil's parameters keep the same as the simulation, and the coil's liftoff is 0.5 mm.

For the MFL signal, the excitation uses permanent magnetic magnetization, which is quasi-static. For the EMAT signal, the excitation frequency is 2 MHz. Second, the MFL signal

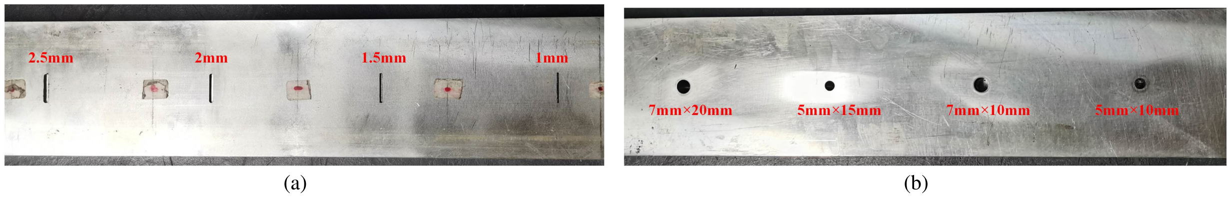

Fig. 14. Steel specimen with surface cracks and blind holes. (a) Top view. (b) Bottom view.

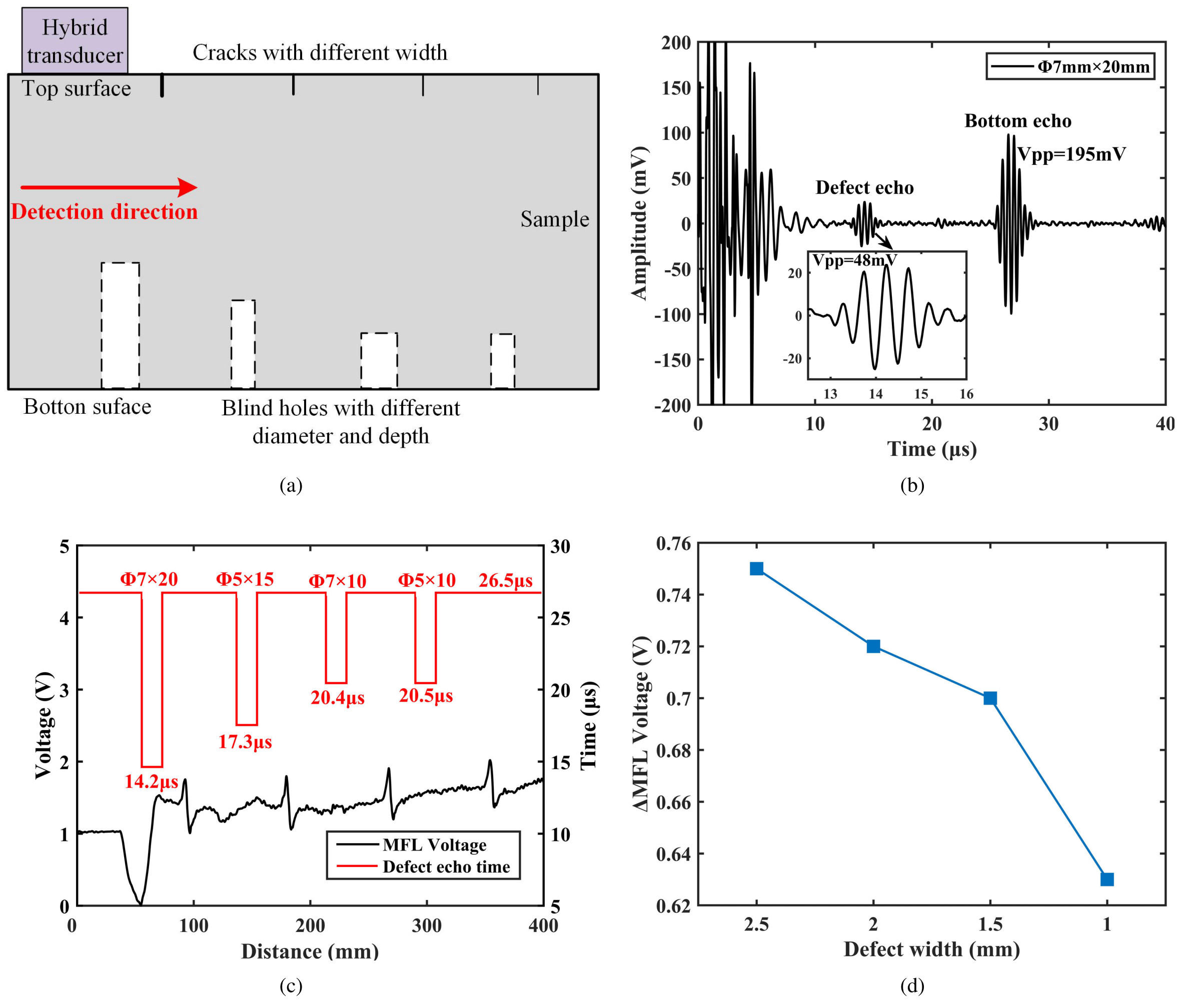

Fig. 15. Experimental results for surface and internal defects. (a) Distribution of surface defects and blind holes. (b) EMAT voltage signal of $\Phi 7 \times 20$ mm blind hole. (c) MFL voltage and defect echo time. (d) ΔMFL voltage with different widths.

is picked up by the Hall sensor, while the ultrasonic signal (generated by the EMAT) is received by the spiral coil; they have different spatial positions. Hall sensors have a bandwidth of 20 KHz, and the high-frequency magnetic field (2 MHz) generated by the EMAT has little effect on the Hall sensor. Therefore, the proposed hybrid transducer can effectively detect both the MFL signal and the EMAT signal.

A. MFL Detection Results Utilizing Hybrid Transducer

To evaluate the MFL detection capability of the hybrid transducer, three types of defects are machined on a 10-mm-thick plate, as shown in Fig. 12(a). They are cracks of identical depth and width but different lengths (18, 16, 14, and 12 mm), cracks of the same length and width but different depths (4, 3, 2, and 1 mm), cracks with identical length, width, and depth but different angles (15°, 30°, 60°, and 75°). The defects with oil adhering to the inside of the pipeline are shown in Fig. 12(b) and (c).

Fig. 13 presents the experimental results for different defects in steel plate and pipeline. As shown in Fig. 13, Bx and Bz have a consistent linear variation rule for different angles, different depths, and different lengths of defects. Fig. 13(c) and (d) shows that Bz changes significantly with defect angle and depth. As the MFL signal is amplified by a factor of approximately 22, the Hall sensor has a sensitivity of 100 mV/mT. For example, taking the experimental data $\Delta Bz = 0.63$ V in Table III, the actual z-direction leakage field is calculated by (8). The voltage variations ΔBx and ΔBz for

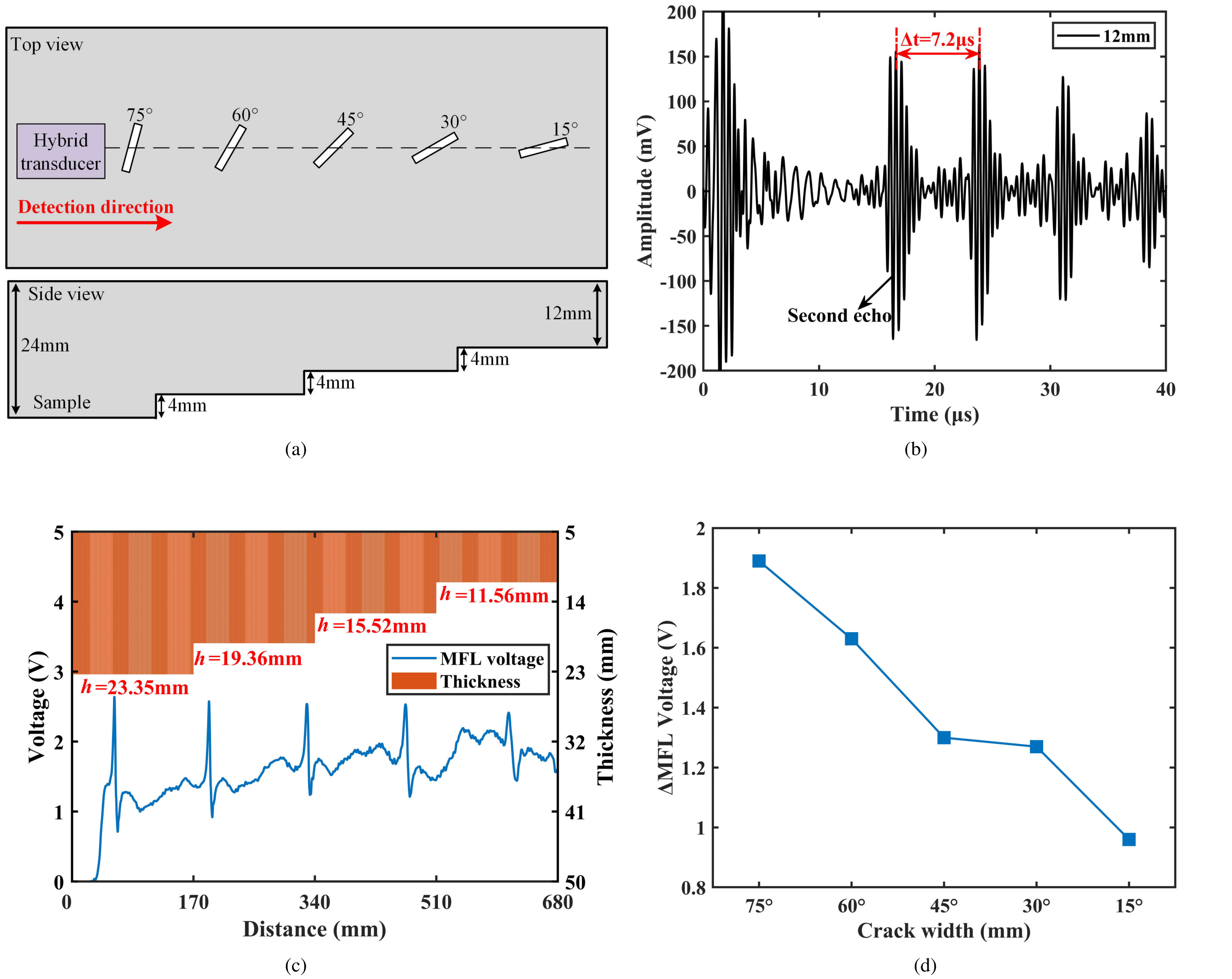

Fig. 16. Experimental results for surface and bottom thinning defects. (a) Distribution of surface defects and bottom thinning defects. (b) EMAT voltage signal of 12 mm thickness. (c) MFL voltage and specimen thickness. (d) ΔMFL voltage with different angles.

the different defect signals are given in Table III. As shown in Table III, the proposed hybrid transducer has a high sensitivity for defects of different angles, depths, and lengths. When the defect is approximately parallel to the transducer (15°), the minimum ΔBz voltage of the transducer can achieve 0.63 V. Fig. 13(e) shows that the proposed hybrid transducer can successfully detect defects inside the oil-containing pipeline

$$\boldsymbol{B}_z = \frac{0.63\ \mathrm{V}}{22 \times 0.1\ \mathrm{V/mT}} = 0.286\ \mathrm{mT}. \tag{8}$$

B. EMAT and MFL Results Utilizing Hybrid Transducer

1) Surface and Internal Defects Detection: To evaluate the detection ability of the hybrid transducer to surface and internal defects, we have designed a 40-mm-thick steel specimen containing four surface cracks with dimensions of 10 mm in length, 1 mm in depth, and 1, 1.5, 2, and 2.5 mm in width. It also has four blind holes at the bottom of the specimen with sizes of 5 mm in diameter, 10 mm and 15 mm in depth, 7 mm in diameter, and 10 and 20 mm in depth, as shown in Fig. 14(a) and (b).

Fig. 15 shows the results of the hybrid transducer in detecting surface and internal defects. Fig. 15(a) represents the distribution of defects in the specimen. When the transducer is placed on the top surface of the specimen and swept in the detection direction, the hybrid transducer will receive the EMAT voltage signal (which carries the internal defect information) and the MFL signal (which carries the surface defect information), as shown in Fig. 15(b) and (c), respectively. Additional EMAT voltage signals are shown in Fig. A2 in the Appendix (see the Supplementary Material). Fig. 15(d) shows that the ΔMFL voltage signal increases with increasing defect width. Table IV provides the detection results of surface defects and bottom defects. Combined with Table IV and Fig. 10, it can be seen that the simulation agrees with the experimental findings. For the same depth of the blind hole in Table IV, the larger the diameter, the higher the SNR of the defect echo. On the other hand, a deeper defect tends to have a shorter echo time, and the maximum bottom defect SNR is 21.1 dB. The hybrid transducer is also highly sensitive to surface defects, and the ΔMFL voltage can reach 0.63 V for a surface defect of 10 mm in length, 1 mm in depth, and 1 mm in width.

The above results show that the proposed hybrid transducer is capable of detecting both surface and internal defects in the specimen with high detection accuracy. No significant electromagnetic interference between the MFL signal and the ultrasonic signal has been found, and defects can be distinguished by two groups of signals.

2) Surface and Bottom Thinning Defects Detection: Fig. 16 shows the results of the hybrid transducer in detecting surface and bottom thinning defects. Fig. 16(a) shows a diagram of the steel specimen, which contains the surface defect with identical length, width, and depth but different angles (75°, 60°, 45°, 30°, and 15°), and bottom thinning defects with 20, 16, and 12 mm, where the reference thickness of this specimen is 24 mm. Fig. 16(b) and (c) shows the EMAT voltage signals and MFL voltage signals obtained by sweeping the hybrid transducer along the detection direction [additional EMAT voltage signals are shown in Fig. A3 in the Appendix (see the Supplementary Material)]. According to (6), the thickness of the sample at the current position can be estimated by calculating the time of adjacent echoes Δt. Fig. 16(d) shows the ΔMFL voltage for surface defects with different angles. Table V presents the measurement results of surface defects and bottom thinning defects. It can be seen from Table V that the proposed transducer is capable of detecting both surface and bottom thinning defects simultaneously, the minimum error of thickness measurement is 2.7% and the minimum detectable surface defect angle is 15°. Even if the defect is close to parallel to the magnetization direction (15°), the hybrid transducer still provides good defect detection sensitivity, with a minimum ΔMFL voltage of 0.93 V.

V. Conclusion

In this article, a multiphysical detection system has been presented based on the MFL-EMAT dual fusion mechanism for detecting surface and internal defects simultaneously. The feasibility of the method has been analyzed by simulation and experiment. The conclusions can be drawn as follows.

1) The proposed system overcomes the drawbacks and limitations of the traditional single detection method. The hybrid transducer combines the magnetic fields in the MFL and EMAT to improve the detection efficiency of the detection system without increasing the spatial structure of the transducer.
2) The MFL voltage signal with surface defects is analyzed using the steady-state analysis method, while the ultrasonic wave signal with internal defects is analyzed by applying the time-domain analysis method. These two different types of signals are isolated directly without interference.
3) Experiment results have shown that the hybrid sensor has good detection accuracy and is able to simultaneously detect surface defects of 10 mm in length, 1 mm in width and depth, the blind hole of Φ5 mm with a depth of 25% thickness, and bottom thinning defect with a minimum thickness of 12 mm.

In the future, we will promote the application of this system in the field of pipe detection.

Acknowledgment

Qin Tang, Bin Gao, Gaige Ru, and Guixin Qin are with the School of Automation Engineering, University of Electronic Science and Technology of China, Chengdu 611731, China (e-mail: 202111060929@std.uestc.cn; bin_gao@uestc.edu.cn).

Wai Lok Woo is with the Department of Computer and Information Sciences, Northumbria University, NE1 8ST Newcastle upon Tyne, U.K. (e-mail: wailok.woo@northumbria.ac.uk).

Shiqiang Jiang is with Sichuan Deyuan Pipeline Technology Company Ltd., Chengdu 610041, China (e-mail: davidjiang@deyuanpipe.com).

Dajiang Chen is with CNOOC China Ltd., Zhanjiang 524057, China (e-mail: chendj2@cnooc.com.cn).

Jingwei Li is with CNPC CHUANQIN Drilling Engineering Company Ltd., Chengdu 610036, China (e-mail: lijwei_sc@cnpc.com.cn).

Ju Cheng is with the PipeChina West East Gas Pipeline Company Si Chuan to Eastern China Gas Transmission Pipeline Co.Ltd, Wuhan 430074, China (e-mail: chengju@pipechina.com.cn).

References

[1] M. Gupta, M. Khan, R. Butola, and R. Singari, “Advances in applications of non-destructive testing (NDT): A review,” *Adv. Mater. Process. Technol.*, vol. 8, no. 2, pp. 2286–2307, Apr. 2022.

[2] S. K. Dwivedi, M. Vishwakarma, and P. A. Soni, “Advances and researches on non destructive testing: A review,” *Mater. Today, Proc.*, vol. 5, no. 2, pp. 3690–3698, 2018.

[3] A. Zolfaghari, A. Zolfaghari, and F. Kolahan, “Reliability and sensitivity of magnetic particle nondestructive testing in detecting the surface cracks of welded components,” *Nondestruct. Test. Eval.*, vol. 33, no. 3, pp. 290–300, Jul. 2018.

[4] S. She, Y. Chen, Y. He, Z. Zhou, and X. Zou, “Optimal design of remote field eddy current testing probe for ferromagnetic pipeline inspection,” *Measurement*, vol. 168, Jan. 2021, Art. no. 108306.

[5] S. Xie et al., “Features extraction and discussion in a novel frequency-band-selecting pulsed eddy current testing method for the detection of a certain depth range of defects,” *NDT E Int.*, vol. 111, Apr. 2020, Art. no. 102211.

[6] X. Yuan et al., “Novel phase reversal feature for inspection of cracks using multi-frequency alternating current field measurement technique,” *Mech. Syst. Signal Process.*, vol. 186, Mar. 2023, Art. no. 109857.

[7] J. Ge, N. Yusa, and M. Fan, “Frequency component mixing of pulsed or multi-frequency eddy current testing for nonferromagnetic plate thickness measurement using a multi-gene genetic programming algorithm,” *NDT E Int.*, vol. 120, Jun. 2021, Art. no. 102423.

[8] X. Peng, U. Anyaoha, Z. Liu, and K. Tsukada, “Analysis of magnetic-flux leakage (MFL) data for pipeline corrosion assessment,” *IEEE Trans. Magn.*, vol. 56, no. 6, pp. 1–15, Jun. 2020.

[9] F. Honarvar and A. Varvani-Farahani, “A review of ultrasonic testing applications in additive manufacturing: Defect evaluation, material characterization, and process control,” *Ultrasonics*, vol. 108, Dec. 2020, Art. no. 106227.

[10] A. C. Kubrusly, L. Kang, I. S. Martins, and S. Dixon, “Unidirectional shear horizontal wave generation by periodic permanent magnets electromagnetic acoustic transducer with dual linear-coil array,” *IEEE Trans. Ultrason., Ferroelectr., Freq. Control*, vol. 68, no. 10, pp. 3135–3142, Oct. 2021.

[11] J. Tkocz and S. Dixon, “Electromagnetic acoustic transducer optimisation for surface wave applications,” *NDT E Int.*, vol. 107, Oct. 2019, Art. no. 102142.

[12] G. Dobmann, F. Niese, H. Willems, and A. Yashan, “Wall thickness measurement sensor for pipeline inspection using EMAT technology in combination with pulsed eddy current and MFL,” *Non-Destruct Test Aust.*, vol. 45, pp. 84–87, Jan. 2008.

[13] S. Wang, P. Zhao, Z. Qu, and K. Wang, “A new system for defects inspection of boiler water wall tubes using a combination of EMAT and MFL,” in *Proc. IEEE Far East NDT New Technol. Appl. Forum (FENDT)*, Jul. 2018, pp. 65–69.

[14] H. Willems, B. Jaskolla, T. Sickinger, A. Barbian, and F. Niese, “A new ILI tool for metal loss inspection of gas pipelines using a combination of ultrasound, eddy current and MFL,” in *Proc. 8th Int. Pipeline Conf.*, Jan. 2010, pp. 557–564.

[15] J. Chang, Z. Chu, X. Gao, A. I. Soldatov, and S. Dong, “A magnetoelectric-ultrasonic multimodal system for synchronous NDE of surface and internal defects in metal,” *Mech. Syst. Signal Process.*, vol. 183, Jan. 2023, Art. no. 109667.

[16] G. Ru, B. Gao, D. Liu, Q. Ma, H. Li, and W. L. Woo, “Structural coupled electromagnetic sensing of defects diagnostic system,” *IEEE Trans. Ind. Electron.*, vol. 70, no. 1, pp. 951–964, Jan. 2023.

[17] V. V. Mishakin, V. A. Klyushnikov, A. V. Gonchar, and M. Kachanov, "On assessing damage in austenitic steel based on combination of the acoustic and eddy current monitoring," *Int. J. Eng. Sci.*, vol. 135, pp. 17–22, Feb. 2019.

[18] X. Yin et al., "A combined inductive and capacitive non-destructive evaluation technique using a single spiral coil sensor," *IEEE Sensors J.*, vol. 21, no. 16, pp. 18187–18196, Aug. 2021.

[19] T. Zhu, M. Mwelango, X. Yin, X. Yuan, W. Li, and G. Chen, "A novel dual-mode sensor for the detection of interface flaw in 'insulator-conductor' composite structures," *IEEE Sensors J.*, vol. 23, no. 5, pp. 4568–4576, Mar. 2023.

[20] H. Li et al., "Multiphysics structured eddy current and thermography defects diagnostics system in moving mode," *IEEE Trans. Ind. Informat.*, vol. 17, no. 4, pp. 2566–2578, Apr. 2021.

[21] M. Toharaand and Y. Gotoh, "Inspection method of outer side defect in ferromagnetic steel tube by insertion-type electromagnetic sensor using square wave alternating magnetic field with DC bias," *IEEE Trans. Magn.*, vol. 57, no. 2, pp. 1–5, Feb. 2021.

[22] W. Li, X. Yuan, G. Chen, J. Ge, X. Yin, and K. Li, "High sensitivity rotating alternating current field measurement for arbitrary-angle underwater cracks," *NDT E Int.*, vol. 79, pp. 123–131, Apr. 2016.

[23] Z. Chu et al., "Enhanced resonance magnetoelectric coupling in (1–1) connectivity composites," *Adv. Mater.*, vol. 29, no. 19, May 2017, Art. no. 1606022.

[24] Z. Chu, Z. Jiang, Z. Mao, Y. Shen, J. Gao, and S. Dong, "Low-power eddy current detection with 1–1 type magnetoelectric sensor for pipeline cracks monitoring," *Sens. Actuators A, Phys.*, vol. 318, Feb. 2021, Art. no. 112496.

[25] B. Liang, Z. Li, G. Zhai, R. Yang, X. Zhang, and S. Dixon, "Enhancing the lift-off performance of EMATs by applying an Fe_3O_4 coating to a test specimen," *IEEE Trans. Instrum. Meas.*, vol. 72, pp. 1–4, 2023.

[26] R. Urayama, T. Uchimoto, and T. Takagi, "Application of EMAT/EC dual probe to monitoring of wall thinning in high temperature environment," *Int. J. Appl. Electromagn. Mech.*, vol. 33, nos. 3–4, pp. 1317–1327, Oct. 2010.

[27] W. Guo, B. Gao, G. Yun Tian, and D. Si, "Physic perspective fusion of electromagnetic acoustic transducer and pulsed eddy current testing in non-destructive testing system," *Phil. Trans. Roy. Soc. A, Math., Phys. Eng. Sci.*, vol. 378, no. 2182, Oct. 2020, Art. no. 20190608.

[28] X. Zhao et al., "Performance degradation detection of 12CrMoV steel by magneto-acoustic compound inspection method," *NDT E Int.*, vol. 124, Dec. 2021, Art. no. 102525.

[29] Z. Duan et al., "Quantitative sizing of compound location defects based on PECT-EMAT hybrid testing methods," *Mech. Syst. Signal Process.*, vol. 178, Oct. 2022, Art. no. 109267.

[30] S. Xie, M. Tian, P. Xiao, C. Pei, Z. Chen, and T. Takagi, "A hybrid nondestructive testing method of pulsed eddy current testing and electromagnetic acoustic transducer techniques for simultaneous surface and volumetric defects inspection," *NDT E Int.*, vol. 86, pp. 153–163, Mar. 2017.

[31] Z. Liu et al., "Numerical decoupling study of EMAT testing signal for ferromagnetic materials," *IEEE Sensors J.*, vol. 20, no. 7, pp. 3476–3486, Apr. 2020.

[32] X. Wang, X. Wu, J. Xu, and H. Ba, "Study on the lift-off effect on MFL signals with magnetic circuit model and 3D FEM," *Insight-Non-Destructive Test. Condition Monitor.*, vol. 54, no. 9, pp. 505–510, Sep. 2012.

[33] R. Thompson, "Physical principles of measurements with EMAT transducers," in *Physical Acoustics*, vol. 19, R. Thurston and A. D. Pierce, Eds. Cambridge, MA, USA: Academic Press, 1990, pp. 157–200.

[34] R. Ribichini, F. Cegla, P. B. Nagy, and P. Cawley, "Experimental and numerical evaluation of electromagnetic acoustic transducer performance on steel materials," *NDT E Int.*, vol. 45, no. 1, pp. 32–38, Jan. 2012.

[35] M. Hirao and H. Ogi, *Electromagnetic Acoustic Transducers, Noncontacting Ultrasonic Measurements using EMATs* (Springer Series in Measurement Science and Technology). Berlin, Germany: Springer, 2017, pp. 21–79.

[36] H. Sun, R. Urayama, T. Uchimoto, T. Takagi, and M. Hashimoto, "Small electromagnetic acoustic transducer with an enhanced unique magnet configuration," *NDT E Int.*, vol. 110, Mar. 2020, Art. no. 102205.

Qin Tang received the M.Sc. degree from Nanchang Hangkong University, Nanchang, China, in 2021. She is currently pursuing the Ph.D. degree in electromagnetic nondestructive evaluation with the University of Electronic Science and Technology of China, Chengdu, China.

Her main research interest is electromagnetic multiphysics fusion detection strategy.

Bin Gao (Senior Member, IEEE) received the B.Sc. degree in communications and signal processing from Southwest Jiaotong University, Chengdu, China, in 2005, and the M.Sc. (Hons.) degree in communications and signal processing and the Ph.D. degree from Newcastle University, Newcastle upon Tyne, U.K., in 2006 and 2011, respectively.

From 2011 to 2013, he worked as a Research Associate with Newcastle University, on wearable acoustic sensor technology. He is currently a Professor with the School of Automation Engineering, University of Electronic Science and Technology of China (UESTC), Chengdu. He is also a very active reviewer for many international journals and long-standing conferences. He has coordinated several research projects from the National Natural Science Foundation of China. His research interests include electromagnetic and thermography sensing, machine learning, and nondestructive testing and evaluation, and he actively publishes in these areas.

Gaige Ru received the M.Sc. degree in control science and engineering from Anhui Polytechnic University, Wuhu, China, in 2019. He is currently pursuing the Ph.D. degree with the University of Electronic Science and Technology of China, Chengdu, China.

His research mainly focuses on eddy current testing and magnetic flux leakage testing and instrumentation manufacturing. His research interests include smart sensors and system design for pipeline inspection.

Guixin Qin received the B.Sc. degree from the University of Electronic Science and Technology of China (UESTC), Chengdu, China, in 2021, where he is currently pursuing the M.Sc. degree in the School of Automation Engineering.

His research interests primarily focus on physics-informed machine learning and nondestructive testing.

Wai Lok Woo (Senior Member, IEEE) received the B.Eng. degree in electrical and electronics engineering and the M.Sc. and Ph.D. degrees in statistical machine learning from Newcastle University, Newcastle upon Tyne, U.K., in 1993, 1995, and 1998, respectively.

He was the Director of Research at the Newcastle Research and Innovation Institute and the Director of Operations at Newcastle University. He is currently a Professor of Machine Learning with Northumbria University, Newcastle upon Tyne. He has published more than 400 papers on these topics on various journals and international conference proceedings. His research interests include mathematical theory and algorithms for data science and analytics, artificial intelligence, machine learning, data mining, latent component analysis, multidimensional signal, and image processing.

Dr. Woo is a member of the Institution of Engineering and Technology. He was a recipient of the IEE Prize and the British Commonwealth Scholarship. He serves as an Associate Editor for several international signal processing journals, including *IET Signal Processing*, the *Journal of Computers*, and the *Journal of Electrical and Computer Engineering*.

Shiqiang (David) Jiang received the bachelor's degree from the College of Geophysics and Petroleum Resources, Yangtze University, Jingzhou, China, in 1992, and the M.B.A. degree from the Southwestern University of Finance and Economics (SWUFE), Chengdu, China, in 2002.

In 2007, he founded Deyuan Pipeline Technology Company Ltd., Chengdu. In 2019, he founded the joint Lab for pipeline ILI research and development with the University of Electronic Science and Technology of China (UESTC), Chengdu. He is the CEO of Deyuan Pipeline Technology Company Ltd.

Dajiang Chen was born in 1979. He graduated in thermal energy and power engineering from Guangdong Ocean University, Zhanjiang, China, in 2002.

He is a Senior Engineer of Pipeline Engineering at CNOOC China Ltd., Zhanjiang. His research fields include installation, maintenance, and testing technology management of offshore oil and gas pipelines and single-point mooring systems.

Jingwei Li received the bachelor's degree in petroleum engineering and the bachelor's degree in business administration from the Southwestern University of Finance and Economics (SWUFE), Chengdu, China, in 2001.

He has been working at CNPC CHUANQIN Drilling Engineering Company Ltd., Chengdu, since 2011. His main career fields include pipeline operation, product operation management, pipeline internal anticorrosion and inspection, and natural gas pipeline security.

Ju Cheng was born in October 1983. He graduated from Southwest Petroleum University (SWPU), Chengdu, China.

He is a Senior Engineer with PipeChina West East Gas Pipeline Company Sichuan to Eastern China Gas Transmission Pipeline Company Ltd., Wuhan, China.